



# Load Distribution and Dynamic Response in Torque Split Applications

Süleyman Emre Civan<sup>1,2,\*</sup>  and Cihan Demir<sup>1</sup> <sup>1</sup> Department of Mechanical Engineering, Yildiz Technical University, Barbaros Bulvari, 34349 Istanbul, Turkey<sup>2</sup> Tusas Engine Industries, Inc. (TEI), Esentepe Mahallesi Cevreyolu Bulvari No. 356, 26210 Eskisehir, Turkey\* Correspondence: [suleymancivan@gmail.com](mailto:suleymancivan@gmail.com) or [suleymanemre.civan@tei.com.tr](mailto:suleymanemre.civan@tei.com.tr)

**Abstract:** This study consists of constructing and analyzing gear mathematical models of torque split systems for contact pressure distribution and dynamic transmission error at different gear positions concerning phase angles. According to the method specified in the AGMA 927 standard, load distribution is calculated by considering shaft torsion and bending deformations. Partial contact loss may occur as a result of shaft bending with asymmetric gear positioning on a long shaft. The contact separation can be decreased by reaction force balancing if the driven gears are in the opposite position with respect to the drive gear. In the calculation of the dynamic transmission error of the torque split model, a parametric phase difference for the gear positions is proposed using gear geometry parameters. The variation of the dynamic response according to the change in the parametric phase angle in the torque split system is analyzed for the same values of each gear. Small changes in the phase values change the system response significantly. To obtain lower dynamic transmission error amplitude, the phase difference and gear positions are examined. The contact pressure distribution is validated by the finite element method, and the dynamic transmission error is compared with the experimental study in the literature.

**Keywords:** spur gear; phase difference; torque split; nonlinear gear dynamics; shaft bending



**Citation:** Civan, S.E.; Demir, C. Load Distribution and Dynamic Response in Torque Split Applications. *Machines* **2022**, *10*, 1218. <https://doi.org/10.3390/machines10121218>

Academic Editor: Davide Astolfi

Received: 12 November 2022

Accepted: 12 December 2022

Published: 15 December 2022

**Publisher's Note:** MDPI stays neutral with regard to jurisdictional claims in published maps and institutional affiliations.



**Copyright:** © 2022 by the authors. Licensee MDPI, Basel, Switzerland. This article is an open access article distributed under the terms and conditions of the Creative Commons Attribution (CC BY) license (<https://creativecommons.org/licenses/by/4.0/>).

## 1. Introduction

The gear system is a key element of power transmission systems in aerospace, automotive, and rail applications in terms of achieving the required speed and torque ratio from input to output. Gear vibration has an important place in drivetrain systems due to noise and durability issues. Gear systems generate dynamic forces that are much higher than static forces in the gear pair under operating conditions. These high-frequency dynamic forces are transmitted through the bearings, producing noise in the system. In addition, variable forces reduce the fatigue life of transmission elements. For this reason, gear dynamics are important in the design of a quiet and durable gear system. Most studies in the literature have been performed on gear pairs. However, the effects of systems such as torque split and idler gear in torque-transferred gear mechanisms should also be considered.

Some studies involving the load distribution and gear pair stiffness for the gear pair can be given as follows; Eritenel and Parker [1] investigated the force and torque distribution, which is non-uniformly distributed along the gear width, in helical gear pairs, taking into account the partial tooth contact loss. Elastic deformation components in the system are not formulated in this study. Yuan et al. [2] used the Timoshenko beam theory to find shaft bending along the width of the gear. The displacements at the gear pair contact are investigated by considering the gear width in slices. The linear and time-dependent gear pair stiffness modeling method finds the dynamic transmission error.

Yuan et al. [3] worked on a hybrid model with lumped mass parameters with loaded tooth contact analysis in cylindrical gears. In addition to the effect of the error along the face width on the loading, the effects of damping and helix angle in the gear pair are investigated. Wang et al. [4] considered the gear in slices along the width, and the variation

of gear pair stiffness with shaft misalignment and crowning is investigated. The stiffness in the side slices against the relative motion along the face width is taken into account. An iterative loop is established to determine whether there is tooth contact or not, by defining an initial value for the deformation in the gear pair and comparing it with the micro-modification and the misalignment value in the shaft. Thus, the contact status for each slice is examined.

Some important studies on gear pair dynamics can be given as follows; Kahraman et al. [5] developed a gear-rotor dynamics model for a gear pair taking into account the compliance of the bearings and the axial loading of the shaft by inertia. Along with the determination of the critical speed, the unbalanced load, geometric eccentricity, and transmission error drive at the contact point are determined. The natural frequency transition due to bearing stiffness is investigated for three different shaft lengths to evaluate rigidity and flexibility. Ma et al. [6] examined the variation of the system dynamics with different addendum coefficients, amounts of tip relief, and profile shifts. The system is modeled without backlash. In the system responses, it is stated that while it is sufficient to minimize the static transmission error from peak to peak in the gear pair operating at high frequencies, the tip relief at low frequencies should be determined according to the gear parameters and system response. Dai and Parker [7] established a hybrid model in which the tooth contact force is taken from the finite elements and used in the analytical vibration model. The partial loss of the contact state is obtained with finite elements, and the force deformation function is used for dynamic modeling. Han et al. [8] worked on tooth contact analysis by taking the misalignment caused by the assembly, production, and system deformations in the helical gear pair as variables along the gear width. Optimization is conducted by a genetic algorithm to minimize the static transmission error and variance of micro-modifications along the profile and width. Finally, the dynamic transmission error in the system with 8 degrees of freedom is investigated at different contact misalignments. Xiong and Gao [9] dynamically modeled the system by considering the non-linear bearing motion, gear pair eccentricity, gear friction, and gear system motion in torsional and translational planes. Gear pair stiffness is determined by the potential energy method. Inalpolat et al. [10] investigated the variation of dynamic transmission error and dynamic gear pair force by giving a certain ratio of pitch error to a tooth in a gear pair with the same number of teeth. The measurement results are compared with the gear pair with relatively less pitch error. It is observed that shaft harmonics increased, and harmonics are obtained in proportion to the number of teeth of the harmonics in the gear pair. Profile errors caused by manufacturing defects vary with processing quality. Therefore, the no-load transmission error is defined by the gear quality. This can be simulated with some assumptions as the resultant of several sine curves. In addition, statistical studies can be performed for deviations from the actual position in profile error [11,12].

Previous studies on gear dynamics in systems with three or more gears are as follows: Kahraman [13] designed three helical gears in two different models with a torque split and an idle gear. He studied the torsional, axial, and oscillating motion of the system for fixed gear pair stiffness and studied the effect of the natural frequency and helix angle and phase difference, and the load on tooth contact and bearings. The static transmission error is given to the system as a sine wave as an excitation. The responses of the system, which indicate the phase angle change according to the odd–even number of teeth, are studied. Chen et al. [14] developed a four-stage helicopter gear model with a hybrid approach using the finite element method and the lumped mass method. Shaft parameters such as the shaft's inner diameter, outer diameter, and length are included in the dynamic model. Nina [15] conducted an experimental comparison study by establishing the numerical model of the noise levels in the spur, helical, and spiral bevel gear mechanisms in the helicopter's main gearbox as a quasi-static system. Dynamic responses are researched by determining the phase angle in the torque split model. Brethee et al. [16] modeled the helical gear pair using 18 degrees of freedom and examined the system responses both analytically and with the experimental setup. In this study, the effects of torsional and lateral movements, time-varying gear pair stiffness, time-varying friction force, and wear

level on the system drive are investigated. As a result of the study, it is stated that there is a correlation between analytical and experimental results. Spectral peaks at gear transition frequencies and sidebands are investigated on wear. It is shown that there are significant increases in the second and third harmonics and sidebands due to wear. Kahraman and Al-shyyab [17] worked on the system, with two of the four gears on three shafts. Gear backlash and static transmission error cause non-linear motion in the system. The stability of the system is studied by reducing the degree of freedom of the system from three to two, defining it from a semi-determined model to a fully definite model, and solving the state space equations with the harmonic balance method. Yavuz et al. [18] found that two of the three gears on three shafts work together. The degree of freedom of the system is reduced to two degrees, taking into account the gear backlash and static transmission error. The responses of the system for torque split and the use of an idle gear with the harmonic balance method are investigated.

Walha et al. [19] modeled the two-stage gear system with 12 degrees of freedom. The system consisted of an input and output load, three shafts, four gears, and bearings. After modeling the system to match the non-linear time-dependent gear pair stiffness, the points where tooth contact loss was studied. Rayleigh damping was used for damping the tooth in the system. The results of the contact loss points in the frequency band were examined. Shi et al. [20] investigated the dynamic conditions in drive, disengagement, and back-to-hit conditions, taking into account friction, time-varying gear pair stiffness, and tooth backlash to investigate system stability. Kim et al. [21] included the bearing deformation in the translational motion to obtain the dynamic response of the system. Thus, the system pressure angle and contact ratio become time-varying parameters in a dynamic model. Gonzalez et al. [22] aimed to reduce the edge contact with the modification given in gear production by determining the shaft misalignment.

Many studies have been carried out on a gear pair in the literature such as friction force, the effect of bearings, time-dependent gear pair stiffness, and damping force. The studies on the gear pair are generally extended by increasing the degrees of freedom for the multi-mesh gear systems. Gear systems with more than one gear pair are important to examine the interactions of the gears with each other. The phase difference between gear meshes is assumed to be a value of  $\pi$  [rad] in the previous studies. This study proposes an exact value over the gear geometry for the dynamic model of the torque split systems. The effect of shaft deflection on the contact load distribution in the gear pair is studied in the literature. As a contribution to this work, load balancing based on the gear-shaft position in the torque split model is proposed. This study is formed in detail by studying the dynamic transmission error and pressure distribution in the torque split model. First, the phase difference between the gear pairs according to the shaft positions is calculated analytically according to the gear geometry. The dynamic transmission error is investigated by establishing a time-dependent nonlinear gear dynamics model with three degrees of freedom of rotation and six degrees of freedom of translational motions of gears, the effect of friction, and three degrees of freedom of shaft rotational motion equations. The time-varying gear pair stiffness previously calculated by Weber Banaschek is used in the model. The transmission error is calculated by numerical integration, and the Runge–Kutta method is used. In Section 2.1, the dynamic transmission error is modeled at different phase angles and shaft positions using the gear parameters from the reference work [23]. The shaft bending and torsional deformations of the gear body are given in Section 2.2, and the load distribution algorithm in AGMA 927 [24] is used similarly. By creating a deformation matrix, a third-degree curve is derived for each roll angle and the force is calculated along the gear width according to the deformation rate. The torque transmitted from the gear pairs causes shaft bending in the torque split model. The deflection direction, which occurs after reaction forces in the pinion, is derived analytically directly depending on the gear position angles. The contact pressure is obtained with half bandwidth according to AGMA 908 [25] standard. In Section 3.1, the dynamic transmission error is validated by comparing the measured results [26] for the gear pair with our simulations. After that, the system

dynamics result in the torque split model, and the effects of the phase difference on the harmonics of each gear pair are studied. In Section 3.2, we aim to show the effect of shaft bending on the torque split model using longer shafts for pressure distribution. Reaction forces at different gear position angles are calculated. Each gear parameter in this study is given the same to show the effect of phase difference in different gear position angles.

### 2. Modeling

The torque split model is investigated under two main headings, namely, system dynamics and contact pressure distribution according to the phase difference. All 3 gears used in the study have the same parameters. A longer shaft is used as in Figure 1b to specifically observe the shaft bending effect in the contact pressure distribution.

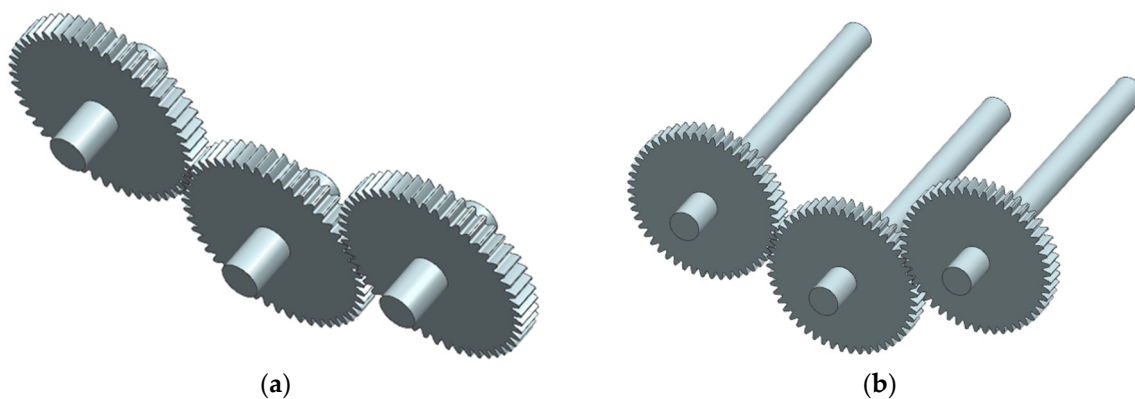


Figure 1. Gear and shaft models for (a) dynamic transmission error and (b) contact pressure distribution studies.

#### 2.1. Gear Dynamics Model

If only one gear pair was used in the system, the motion of each gear would be assumed on the line of action. However, in the system consisting of three gears to be investigated from different angles, the degrees of freedom are defined in the X and Y directions. When shaft motions are included, 12 degrees of freedom are modeled in dynamic equations, as shown in Figure 2. The degrees of freedom in the X direction are not shown in the figure to avoid complexity. In addition, gear backlash, friction, and time-varying gear pair stiffness are taken into account.

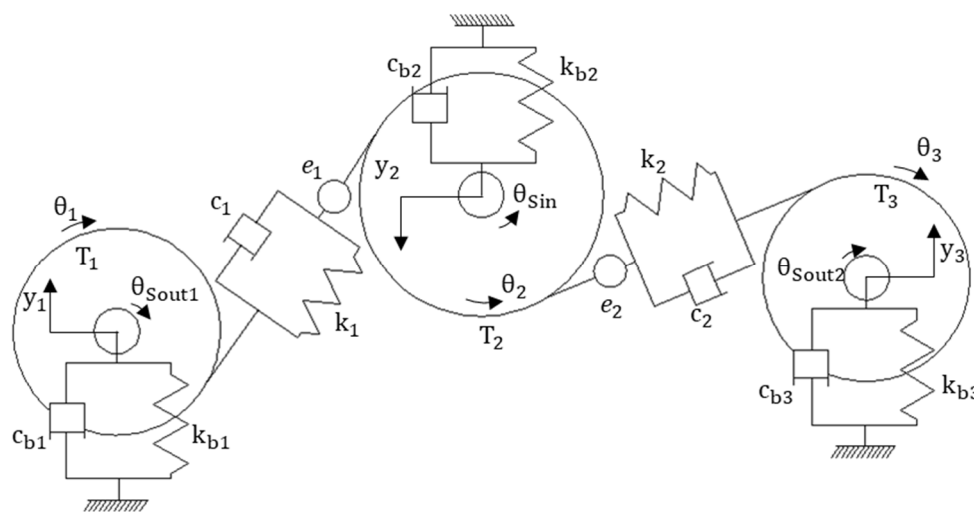
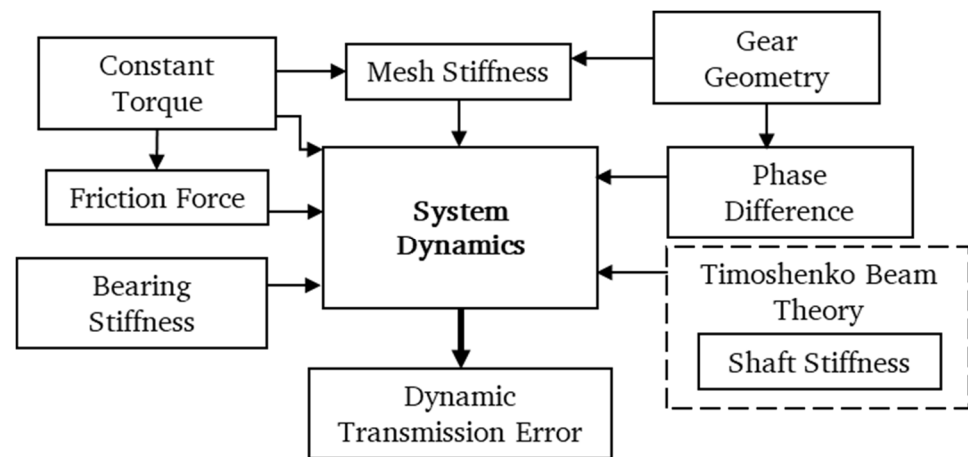


Figure 2. Schematic of the torque split model for 12 degrees of freedom.

The steps given in Figure 3 are followed for dynamic transmission error calculation. Gear pair stiffness and shaft stiffness according to the Weber Banaschek equation are calculated by the finite element method according to the Timoshenko beam theory. The value of  $10^8$  N/m is used for the bearing stiffness in the radial direction. An analytically calculated phase difference according to the geometry is defined between the contact points of both gear pairs. Thus, the time-dependent system response is obtained for both gear pairs.



**Figure 3.** Flow chart for dynamic transmission error calculation.

### 2.1.1. Calculation of Friction Force in the Gear System

Assuming that there is no power loss in the system, the relation between the theoretical input and output powers can be written as in Equation (1).

$$T_2\omega_2 = T_1\omega_2 \frac{Z_2}{Z_1} + T_3\omega_2 \frac{Z_2}{Z_3} \quad (1)$$

Considering the direction change, the X and Y components of the friction force should be determined as positive or negative according to the reference axis. The friction coefficient is usually defined as between 0.03 and 0.07 in the literature. The friction coefficient value of 0.05 is taken as a constant for this study. Equation (2) is taken as an even number before the reference axis and an odd number after the reference axis.  $F_{s_{1a}}$  represents the tooth that is in contact and  $F_{s_{1b}}$  represents the following tooth. The directions of  $F_{s_{1a}}$  and  $F_{s_{1b}}$  will always be opposite each other.

$$F_{s_{1,2}} = (-1)^p \cdot \mu \cdot W_{1,2} \quad (2)$$

We assume that the input torque in the system is constant. The new torque output value at the output is found by taking the difference from the torque value caused by the friction force. First, there is the normal force transmitted in the system. Afterward, the normal force in the transmitted gear is considered to be equal and opposite to the pinion. The new torque value in Equation (3) is obtained for each gear in the torque split model by subtracting the friction force. The equation for the pinion gear takes into account the frictional torque generated by two pairs of gears at the same time. The direction and contact point of the friction force depending on the rotation in a gear pair are shown in Figure 4. The following abbreviations are used for Figure 4: SAP is the start point of the active profile, LPSTC is the lowest point of the active profile, HPSTC is the highest point of the active profile, and EAP is the end of the active profile.

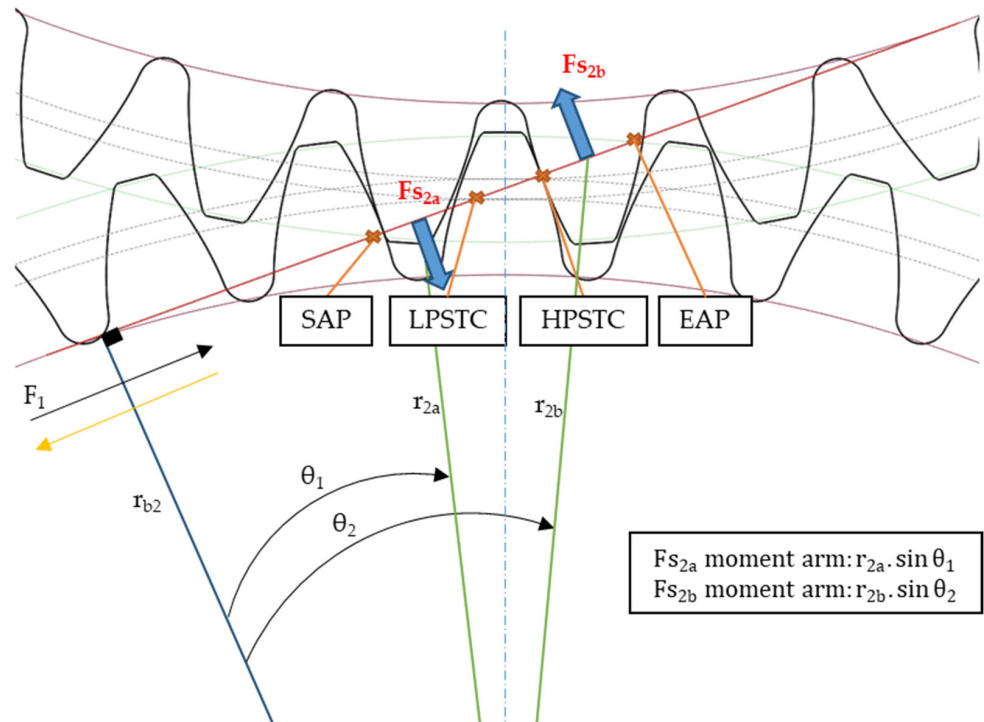


**Figure 4.** Determination of friction torque relative to the contact point.

The directions of the friction force in the torque split model are given in Figure A1 in Appendix A. In addition, the horizontal and vertical angle components are given in Figure A2 so that the components of the loads in the X and Y directions can be taken according to the line of action direction in the torque split model. Only operating pitch circles are specified in the gears for simplicity. The direction of friction force of each tooth pair changes after the centerline along the line of action. Using three gears in the system requires separating force components into X and Y directions. Friction force magnitude peaks in the single tooth region due to force distribution along the line of action and becomes zero at the centerline point. Sliding velocity directly depends on the contact point location on the line of action and its direction also changes going through the centerline. Sliding velocity reaches the maximum value at the start of the active profile point and the end of the active profile points.

$$\begin{aligned}
 T_2 &= F_{n_{\text{new}}} \cdot r_{b2} + F_{s2a} \cdot r_{2a} \cdot \sin(\theta_{2a}) + F_{s2b} \cdot r_{2b} \cdot \sin(\theta_{2b}) \\
 F_{n_{\text{new}}} \cdot r_{b1} &= T_{1_{\text{new}}} + F_{s2a} \cdot r_{1a} \cdot \sin(\theta_{1a}) + F_{s2b} \cdot r_{1b} \cdot \sin(\theta_{1b}) \\
 F_{n_{\text{new}}} \cdot r_{b3} &= T_{3_{\text{new}}} + F_{s2a} \cdot r_{3a} \cdot \sin(\theta_{3a}) + F_{s2b} \cdot r_{3b} \cdot \sin(\theta_{3b})
 \end{aligned} \quad (3)$$

### 2.1.2. Equations of Motion

The friction force in the gear system is modeled by considering the time-dependent gear pair stiffness and the nonlinear effect caused by the backlash. Since the angle between the three gears is also considered, the X and Y directions should be taken separately. Dynamic equations are established by taking into account the rotation of the gears in the X and Y components and the shaft degrees of freedom in the rotational motion.

In gear pairs, it is named angle  $\gamma$  as in Equation (4) to show the angle the line of action makes with the horizontal plane more simply.

$$\begin{aligned}
 \gamma_1 &= \psi_1 - \alpha_{12w} - \pi/2 \\
 \gamma_2 &= \psi_2 - \alpha_{23w}
 \end{aligned} \quad (4)$$

The dynamic transmission error equations, in which the axial displacements are also included in the RZ direction, are obtained as in Equation (5) for two gear pairs.

$$\begin{aligned} p_1 &= r_2\theta_2 - r_1\theta_1 - e_1 + (y_2 - y_1) \sin(\gamma_1) + (x_2 - x_1) \cos(\gamma_1) \\ p_2 &= r_2\theta_2 - r_3\theta_3 - e_2 + (y_2 - y_3) \cos(\gamma_2) + (x_2 - x_3) \sin(\gamma_2) \end{aligned} \quad (5)$$

The equations of motion in the X and Y directions of each gear-shaft mass,

$$\begin{aligned} m_1\ddot{x}_1 + k_{b1}(x_1) + c_{b1}(\dot{x}_1) - c_1(\dot{p}_1) \cos(\gamma_1) - k_1g_1 \cos(\gamma_1) &= 0 \\ m_1\ddot{y}_1 + k_{b1}(y_1) + c_{b1}(\dot{y}_1) - c_1(\dot{p}_1) \sin(\gamma_1) - k_1g_1 \sin(\gamma_1) &= 0 \\ m_2\ddot{x}_2 + k_{b2}(x_2) + c_{b2}(\dot{x}_2) + c_1(\dot{p}_1) \cos(\gamma_1) + k_1g_1 \cos(\gamma_1) + c_2(\dot{p}_2) \sin(\gamma_2) \\ &+ k_2g_2 \sin(\gamma_2) = 0 \\ m_2\ddot{y}_2 + k_{b2}(y_2) + c_{b2}(\dot{y}_2) + c_1(\dot{p}_1) \sin(\gamma_1) + k_1g_1 \sin(\gamma_1) + c_2(\dot{p}_2) \cos(\gamma_2) \\ &+ k_2g_2 \cos(\gamma_2) = 0 \\ m_3\ddot{x}_3 + k_{b3}(x_3) + c_{b3}(\dot{x}_3) - c_2(\dot{p}_2) \sin(\gamma_2) - k_2g_2 \sin(\gamma_2) &= 0 \\ m_3\ddot{y}_3 + k_{b3}(y_3) + c_{b3}(\dot{y}_3) - c_2(\dot{p}_2) \cos(\gamma_2) - k_2g_2 \cos(\gamma_2) &= 0 \end{aligned} \quad (6)$$

The equations of motion in the RZ direction for the 3 shafts,

$$\begin{aligned} J_{\text{Sin}}\ddot{\theta}_{\text{Sin}} + c_{\text{Sin}}(\dot{\theta}_{\text{Sin}} - \dot{\theta}_2) + k_{\text{Sin}2}(\theta_{\text{Sin}} - \theta_2) &= T_2 \\ J_{\text{Sout}1}\ddot{\theta}_{\text{Sout}1} + c_{\text{Sout}1}(\dot{\theta}_{\text{Sout}1} - \dot{\theta}_1) + k_{\text{Sout}1}(\theta_{\text{Sout}1} - \theta_1) &= -T_{1_{\text{new}}} \\ J_{\text{Sout}2}\ddot{\theta}_{\text{Sout}2} + c_{\text{Sout}2}(\dot{\theta}_{\text{Sout}2} - \dot{\theta}_3) + k_{\text{Sout}2}(\theta_{\text{Sout}2} - \theta_3) &= -T_{3_{\text{new}}} \end{aligned} \quad (7)$$

Considering the gear equations  $T_1$  and  $T_3$  output torques are not constant due to friction, time-varying output torque values are included in the dynamic model in Equation (8).

$$\begin{aligned} J_1\ddot{\theta}_1 + c_{\text{Sout}1}(\dot{\theta}_1 - \dot{\theta}_{\text{Sout}1}) + k_{\text{Sout}1}(\theta_1 - \theta_{\text{Sout}1}) - r_1c_1\dot{p}_1 - r_1k_1g_1 \\ = -F_{\text{S}1a} r_{1a} \sin(\theta_{1a}) - F_{\text{S}1b} r_{1b} \sin(\theta_{1b}) \\ J_2\ddot{\theta}_2 + c_{\text{Sin}}(\dot{\theta}_2 - \dot{\theta}_{\text{Sin}}) + k_{\text{Sin}}(\theta_2 - \theta_{\text{Sin}}) + r_2c_1\dot{p}_1 + r_2k_1g_1 + r_2c_2\dot{p}_2 + r_2k_2g_2 \\ = F_{\text{S}1a} r_{2a} \sin(\theta_{2a}) + F_{\text{S}1b} r_{2b} \sin(\theta_{2b}) \\ J_3\ddot{\theta}_3 + c_{\text{Sout}2}(\dot{\theta}_3 - \dot{\theta}_{\text{Sout}2}) + k_{\text{Sout}2}(\theta_3 - \theta_{\text{Sout}2}) - r_3c_2\dot{p}_2 - r_3k_2g_2 \\ = -F_{\text{S}2a} r_{3a} \sin(\theta_{3a}) - F_{\text{S}2b} r_{3b} \sin(\theta_{3b}) \end{aligned} \quad (8)$$

The right-hand side of the equation indicates the time-varying friction losses in the gears.  $J_2$  represents the mass moment of inertia of the pinion and the mass moments of inertia of the  $J_1$  and  $J_3$  driven gears. It is similar to other indices.

There should be some backlash between the gear pair so that it does not jam during the system motion. As the torque in the system increases, tooth contact loss in the line of action decreases. If the torque is not high, tooth contact may be lost and the tooth may hit the following tooth or not contact the mating gear. The nonlinear displacement factor can be obtained as given in Equation (9) with gear dynamic modeling. The nonlinear dynamic factor includes the gear mesh stiffness and backlash. The nonlinear displacement functions  $g_1$  and  $g_2$  for two gear pairs are defined as follows.

$$\begin{aligned} g_1 &\begin{cases} p_1 - b_1, & p_1 > b_1 \\ 0, & -b_1 \leq p_1 \leq b_1 \\ p_1 + b_1, & p_1 < -b_1 \end{cases} \\ g_2 &\begin{cases} p_2 - b_2, & p_2 > b_2 \\ 0, & -b_2 \leq p_2 \leq b_2 \\ p_2 + b_2, & p_2 < -b_2 \end{cases} \end{aligned} \quad (9)$$

### 2.1.3. Phase Difference

In the torque split model, the difference when the two gear pairs come into contact needs to be calculated analytically. Two gear pairs always have the same certain phase difference between them. The position of the first gear pair is assumed to be on the centerline. Afterward, a phase difference in radians is defined at which position the second gear pair is between the contact start and endpoints, and the angle difference between the mesh stiffness inputs is given in the simulation. The radius on the base circle is found by multiplying the radius at any point with the cosine of the pressure angle of that point, as in Equation (10).

$$\begin{aligned} r_b &= r_i \cos \alpha \\ r_p \cos \alpha &= r_w \cos \alpha_w = r_b \end{aligned} \tag{10}$$

The pitch amount is equal to the multiplication of the pi number of the module on the reference circle. It is desired to find the pitch length at any point on the gear as in Figure 5,

$$\begin{aligned} \frac{2\pi}{N} r_p \cos \alpha &= \frac{2\pi}{N} r_w \cos \alpha_w \\ \pi m \cos \alpha &= p' \cos \alpha_w \\ p' &= \frac{\pi m \cos \alpha}{\cos \alpha_w} \end{aligned} \tag{11}$$

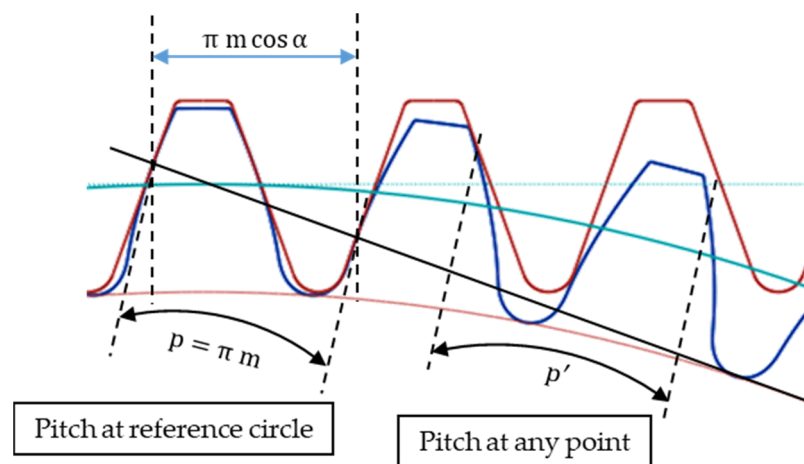


Figure 5. Obtaining pitch at any point.

Vibration damping of gears on each other can be achieved by adjusting the phase angle. As the phase angle changes, torsional vibration decreases, while lateral vibration increases or vice versa. For this, optimization should be performed between 2 planes [27].

The working pressure angle between gears 2 and 3 is

$$\cos \alpha_{23 w} = \frac{r_{b2} + r_{b3}}{O_2 O_3} \tag{12}$$

The working pressure angle between gears 1 and 2 is

$$\cos \alpha_{12 w} = \frac{r_{b1} + r_{b2}}{O_1 O_2} \tag{13}$$

$N'$  is the pitch number between the 1st contact and the 2nd contact, and  $\varphi$  is the phase difference [rad]. The number of the pitch from the first gear pair contact point to the second gear pair contact point as shown in Figure 6 is found in Equation (14) and this number should be rounded down.

$$N' = \left\lfloor \frac{N \cdot \varphi}{2 \pi} \right\rfloor \tag{14}$$



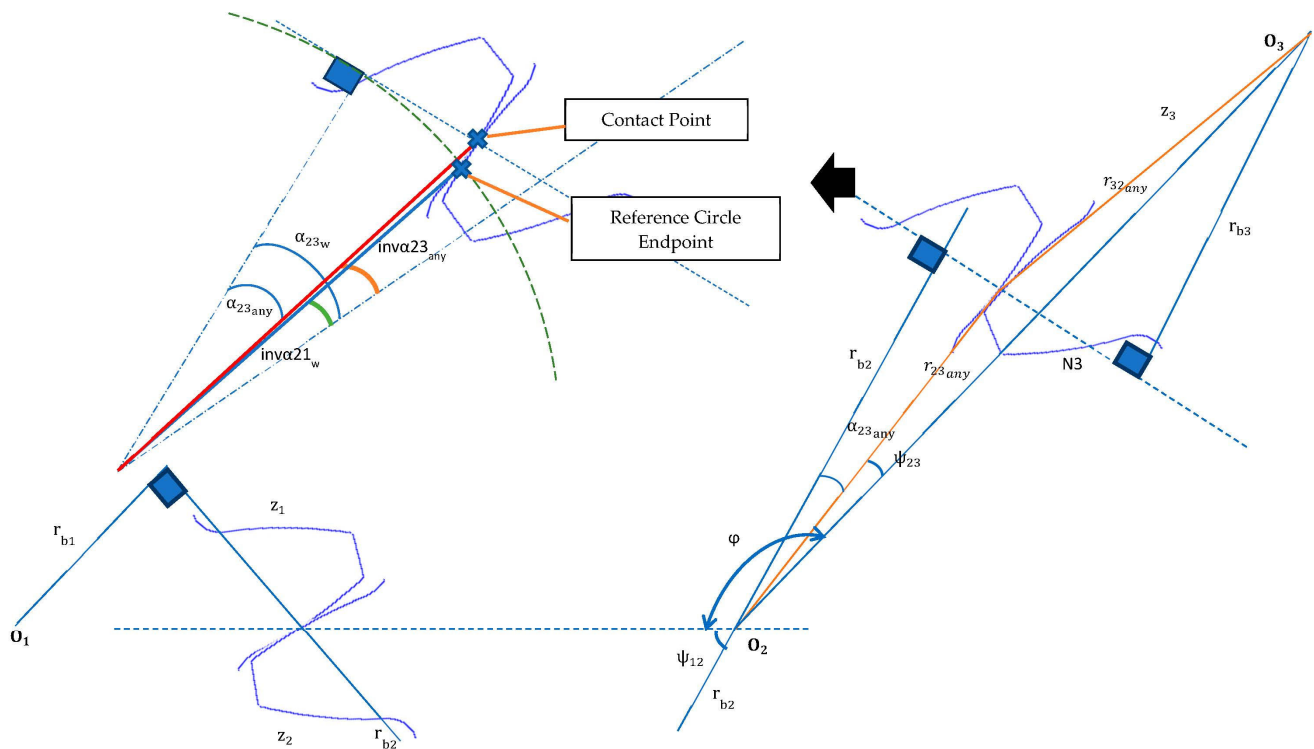


Figure 6. Contact status before centerline.

Equation (15), depending on the angle  $\varphi$ , is obtained by establishing a relation at the pitch endpoint, not the second gear pair contact point.

$$r_{21w} \cdot [(\varphi - \alpha_{23w} + \alpha_{23any}) + (\text{inv } \alpha_{23any} - \text{inv } \alpha_{21w})] = N' \frac{\pi \cdot m \cdot \cos \alpha_p}{\cos \alpha_{21w}} \quad (15)$$

$$\alpha_{23any} = \text{atan} \left( N' \frac{\pi \cdot m \cdot \cos \alpha_{21c}}{\cos \alpha_{21w}} \frac{1}{r_{21w}} - \varphi + \alpha_{23w} + \tan \alpha_{21w} - \alpha_{21w} \right)$$

If the instantaneous pressure angle in gears 2–3 is smaller than the pressure angle in the SAP where the contact starts, the number of pitches is increased by one and the algorithm is repeated starting from the step in Equation (14).

$$\text{If } (\alpha_{23any} < \alpha_{\text{SAP}23}, N', N' + 1) \quad (16)$$

If the pressure angle obtained by Equation (16) is greater than the pressure angle in the SAP, it is taken as the angle of rotation as in Equation (17).

$$\theta_{23any} = \tan \alpha_{23any} \quad (17)$$

Thus, the contact between gears 1–2 and 2–3 is obtained by the phase difference in Equation (18).

$$\varphi = \theta_{21w} - \theta_{23any} \quad (18)$$

## 2.2. System Deformation

The contact pressure distribution calculation algorithm for the gear pair is given in Figure 7. Parametric relations depending on the angle are proposed in this section for the change in contact force at different gear position angles using the same shaft and gear parameters.

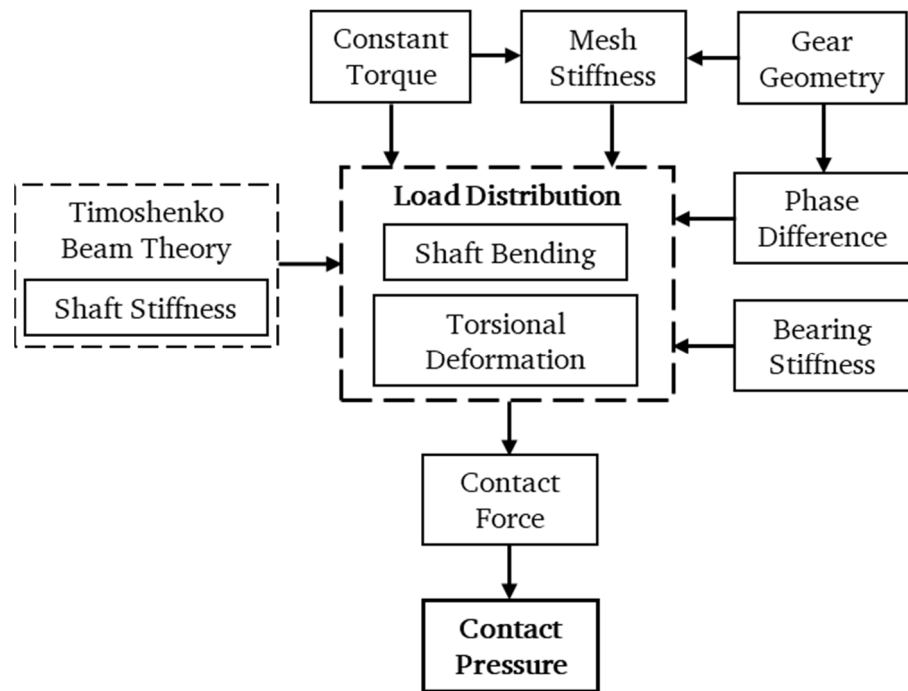


Figure 7. Flow chart used for the pressure distribution of the torque split model.

Bending and torsional displacements of the shaft are calculated by Timoshenko beam theory using the finite element method. The assumptions are as follows:

- The axial direction is not included in spur gears because the axial load is too small.
- The gear shaft is specified with a single stiffness matrix, assuming that it fits tightly on the shaft or is produced in one piece. The gear diameter is assumed as the increase in the diameter of the shaft with the pitch circle.

$K_s$  is the stiffness matrix with 3 degrees of freedom at each node created for the shaft and gear body. By defining more finite elements along the width of the gear, displacements due to deflection are obtained more precisely. The total number of elements is determined by the shaft length and gear width.

$K_b$  is the stiffness matrix of the bearing as point support with axial spring values in X and Y directions, and only the diagonal elements are taken into account. The assembly of the joint points of the bearing and shaft in the stiffness matrix is given in Equation (19). Other elements are ignored, and the bearing is assumed to have no clearance [28].

$$K = K_s + K_b \tag{19}$$

### 2.2.1. Torsional Deformation in the Gear Body

The torsional angle is obtained by iterating the applied load distribution along the gear face width. As shown in Figure 8, the relation of the deformation angle along the gear face width for the uniform load distribution is obtained in Equation (20).

$$\theta = \int_0^L \frac{F_n x r_b}{G J_p} dx = \frac{F_n r_b x^3}{3 G J_p L} \Big|_0^L \tag{20}$$

Torsional deformation,

$$\delta_{\text{torsional}} = r_{\text{any}} \theta \text{ [mm]} \tag{21}$$

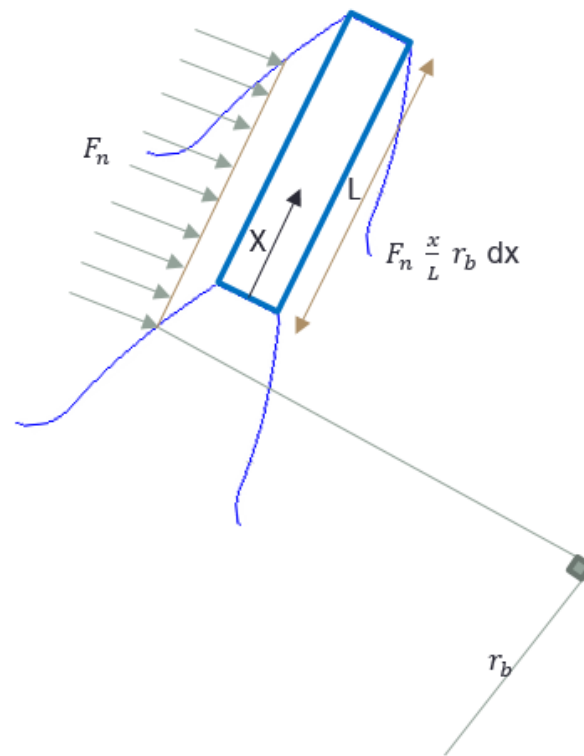


**Figure 8.** Finding the torsional deformation in the RZ direction with uniform loading.

Primarily, torsional deformation is calculated with a uniformly distributed load. Here, the contact force will be non-uniformly distributed due to elastic deformation. After the load distribution is obtained on the surface, the torsional deformation calculation is repeated. The updated torsional deformation angle is found according to the contact status,

$$\theta_{\text{dist}} = \int_0^L \frac{F_n(x)r_b x dx}{G J_p} \tag{22}$$

The torsional deformation along the face width is interpolated with a third-order function in Equation (23).

$$f_{(x)} = ax^3 + bx^2 + cx + d \tag{23}$$

where a, b, c, and d are the function coefficients, and these parameters can be found by deriving the curve. The deformation angle in the RZ direction along the gear width is

$$\theta_{\text{dist}} = \frac{r_b}{G J_p} \int_0^L F_n(x) x dx = \frac{r_b}{G J_p} \int_0^L (ax^4 + bx^3 + cx^2 + dx) dx \tag{24}$$

The amount of deformation of the gear body in the RZ direction obtained by iteration is

$$\delta_{\text{torsional}_{\text{new}}} = r_{\text{any}} \theta \text{ [mm]} \tag{25}$$

### 2.2.2. Shaft Bending

The gear-shaft stiffness matrix is formed by determining the number of elements according to the distance to the bearing center from the gear. The resulting shaft stiffness matrix is inverted and multiplied by the load vector matrix to obtain the displacement at each node as in Equation (26).

$$q_i = [K^{-1}][F_{\text{new}}] \tag{26}$$

when calculating the deflection of the shaft caused by the load on the line of action, the difference in the nodes along the gear width from the minimum to the maximum is taken as in Equation (27).

$$\delta_{\text{bending}} = (q_i - q_{\text{min}}) \quad (27)$$

The deformation on the tooth caused by the load is the same at each node without the system deformation component. Contact separation components such as torsional deformation of the gear body and shaft bending need to add up linearly along the line of action to obtain the deformation matrix. While the bending on the shaft shown in Equation (28) causes a loss of contact between the gear surfaces, the torsional deformation of the gear body changes according to the position of the gear on the shaft.

$$\delta_{\text{total}(i,j)} = \pm \delta_{\text{torsion}(i,j)} - \delta_{\text{bending}(i,j)} \quad (28)$$

After finding the total deformation in the gear pair, the load distribution depending on the roll angle is calculated in Equation (29), similar to in AGMA 927 [24].

$$L_{\delta_i} - L_{\delta_j} = (\delta_i - \delta_j) C_{\gamma m} \quad (29)$$

where  $L_{\delta_i}$  is the load density [N/mm],  $\delta_i$  is the total deformation of the  $i$ th slice in the tooth [ $\mu\text{m}$ ], and  $C_{\gamma m}$  is the contact stiffness. After finding the amount of load at each roll angle, the contact pressure distribution is calculated using the contact half width and load distribution as given in AGMA 908 [25].

### 2.2.3. Tooth Contact Analysis in Torque Split Model

In the torque split model, the angle of the line of action with the horizontal plane in two gear pairs is specified more simply by giving  $\Delta_1$  and  $\Delta_2$  in Equation (30). The reaction forces in the 1st and 3rd gears, where torque is transferred, change as positive or negative according to the positions of the gears. In addition, the direction of the line of action changes according to the position of the gear pair. Therefore, the deflection of the shafts is calculated according to the direction and angle at each position. The same gear parameters are used for each gear in the torque split model to better determine the effect of the phase difference.

$$\begin{aligned} \Delta_1 &= \psi_1 - \alpha_{12w} - \frac{\pi}{2} \\ \Delta_2 &= \frac{\pi}{2} - \psi_2 - \alpha_{23w} \end{aligned} \quad (30)$$

The reaction forces in the torque-transferred gears are divided into X and Y components in Equation (31). Considering that gravity is in the -Y direction,  $m_{(i)}g$ , the weights of gears and shafts are also taken into account.

$$\begin{aligned} R1X &= -Fn_{12} \cos(\Delta_1) \\ R1Y &= -Fn_{12} \sin(\Delta_1) - m_1g \\ R3X &= -Fn_{23} \cos(\Delta_2) \\ R3Y &= Fn_{23} \sin(\Delta_2) - m_3g \end{aligned} \quad (31)$$

The reaction forces in the pinion are in the opposite direction of the reaction forces of the other two driven gears as given in Equation (32).

$$\begin{aligned} R2X &= -R1X - R3X \\ R2Y &= -R1Y - R3Y + m_1g + m_3g - m_2g \end{aligned} \quad (32)$$

While the reaction force in the gear is on the line of action, the reaction force in the pinion is in the opposite direction with the balancing in the two gear pairs. It is used in the shaft bending calculation by taking into account the component of the reaction force in the pinion on the line of action of each gear pair. Thus, the contact pattern with the balancing effect of the system is studied. The angle of the reaction force at the pinion is

$$\phi = \text{atan}\left(\frac{R2Y}{R2X}\right) \quad (33)$$

Equation (34) can be used for the component of the reaction force between gears 1–2. If R2X is a positive value, n is taken as an odd number; otherwise, it is an even number. From this relationship, the component ratio of the reaction force of the pinion in the 1–2 line of action direction is obtained.

$$\begin{aligned} & \text{If } \phi < 0 \\ R2_{12} &= \cos(\pi - \Delta_1 + \phi)(-1)^n \\ & \text{If } \phi > 0 \\ R2_{12} &= \cos(\phi - \Delta_1)(-1)^n \end{aligned} \quad (34)$$

Shaft bending for the gear pair is multiplied by R2<sub>12</sub> to find the deflection in the torque split considering the balancing effect as in Equation (35).

$$\delta_{\text{bending}_{\text{pinion12}}} = (q_i - q_{\text{min}}) R2_{12} \quad (35)$$

The total deflection of the gear pair is obtained in Equation (36) as the sum of the deflections of the pinion and driven gear shafts. This value is taken into account for the deflection in tooth contact analysis of the torque split model.

$$\delta_{\text{bending}_{12}} = \delta_{\text{bending}_{\text{pinion12}}} + \delta_{\text{bending}_{\text{gear12}}} \quad (36)$$

If R2Y is positive, n is taken as an even number; otherwise, it is an odd number. The component ratio of the reaction force of the pinion in the 2-3 line of action direction is

$$\begin{aligned} & \text{If } \phi < 0 \\ R2_{23} &= \cos(\Delta_2 + \phi)(-1)^n \\ & \text{If } \phi > 0 \\ R2_{23} &= \cos(\pi + \phi - \Delta_2)(-1)^n \end{aligned} \quad (37)$$

The total deflection in the gear pair can be obtained by Equation (38) as in the deflection calculation between 2 and 3.

$$\delta_{\text{bending}_{\text{pinion23}}} = (q_i - q_{\text{min}}) R2_{23} \quad (38)$$

The total amount of shaft deformation caused by shaft bending in the gear pair is

$$\delta_{\text{bending}_{23}} = \delta_{\text{bending}_{\text{pinion23}}} + \delta_{\text{bending}_{\text{gear23}}} \quad (39)$$

### 3. Numerical Analysis

In this section, the dynamic response of the torque split model and the variation of the load distribution is given at different gear position angles. Since the phase difference between the two gear pairs in the system dynamic response is affected by small-angle differences between LPSTC and EAP in the contact region, different gear position angles with small increments are used. The gear position angle difference is directly converted to the radian difference between gear pairs and reflected in the dynamic model as a phase difference. The direction of the force is investigated by changing the angle difference between 90 and 180 degrees to emphasize load balancing in tooth surface load distribution. The gear parameters in Table 1 are used to compare the test data in the dynamic transmission error measurement given in the reference studies [17,23].

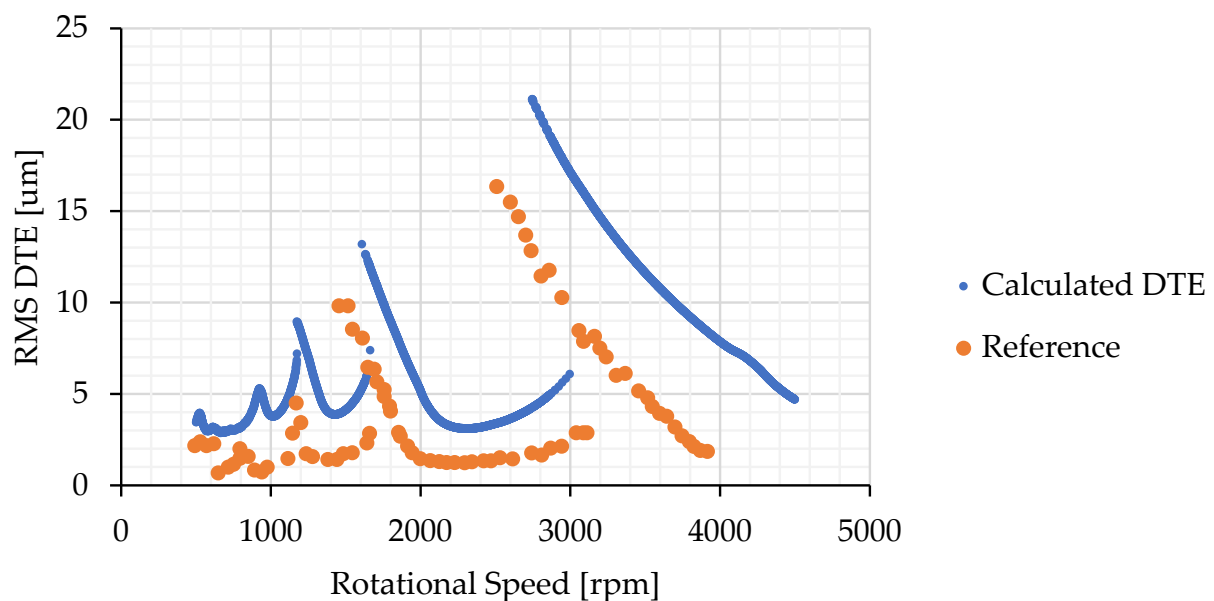
**Table 1.** Test gear parameters used in Refs. [17,23].

	Pinion/Gear
Number of teeth	50
Module	3
Pressure angle [°]	20
Base circle [mm]	140.95
Tip diameter [mm]	156
Root diameter [mm]	140.68
Gear width [mm]	20
Young's modulus [MPa]	206,000
Poisson coefficient	0.3
Center distance [mm]	150
Backlash at the line of action [mm]	0.136
Contact ratio	1.75

### 3.1. System Response in the Torque Split

Experimental data on the dynamic transmission error in the literature are used to validate the system dynamic response in this proposed model using the results from a given study [26]. The test rig type is a mechanical closed power loop for dynamic transmission error measurement from a spur gear pair.

The jump phenomenon occurs when the input speed is close to the resonance speed of the gear system, causing tooth pair separations caused by relative dynamic displacement during gear rotation. When the input velocity is approximately the main and harmonic resonance velocities of the system, the jump during acceleration is not the same as during the deceleration process. The numerical results are compared with the measurement results from the test system. The amplitude jump phenomenon is seen in the back-and-forth sweep shown in Figure 9.

**Figure 9.** Comparison between measured DTE in spur gear pair [26] and calculation.

It can be found that the pattern of dynamic transmission error results matches the experimental results, especially the frequency ranges of harmonics as seen in Figure 9. The

results in Figure 10 are obtained by developing the gear dynamic model and using it for the torque split model. Amplitudes of DTE are specified by unloaded static transmission error and shift to higher values with higher manufacturing errors. We may obtain closer results by decreasing the unloaded static transmission error.

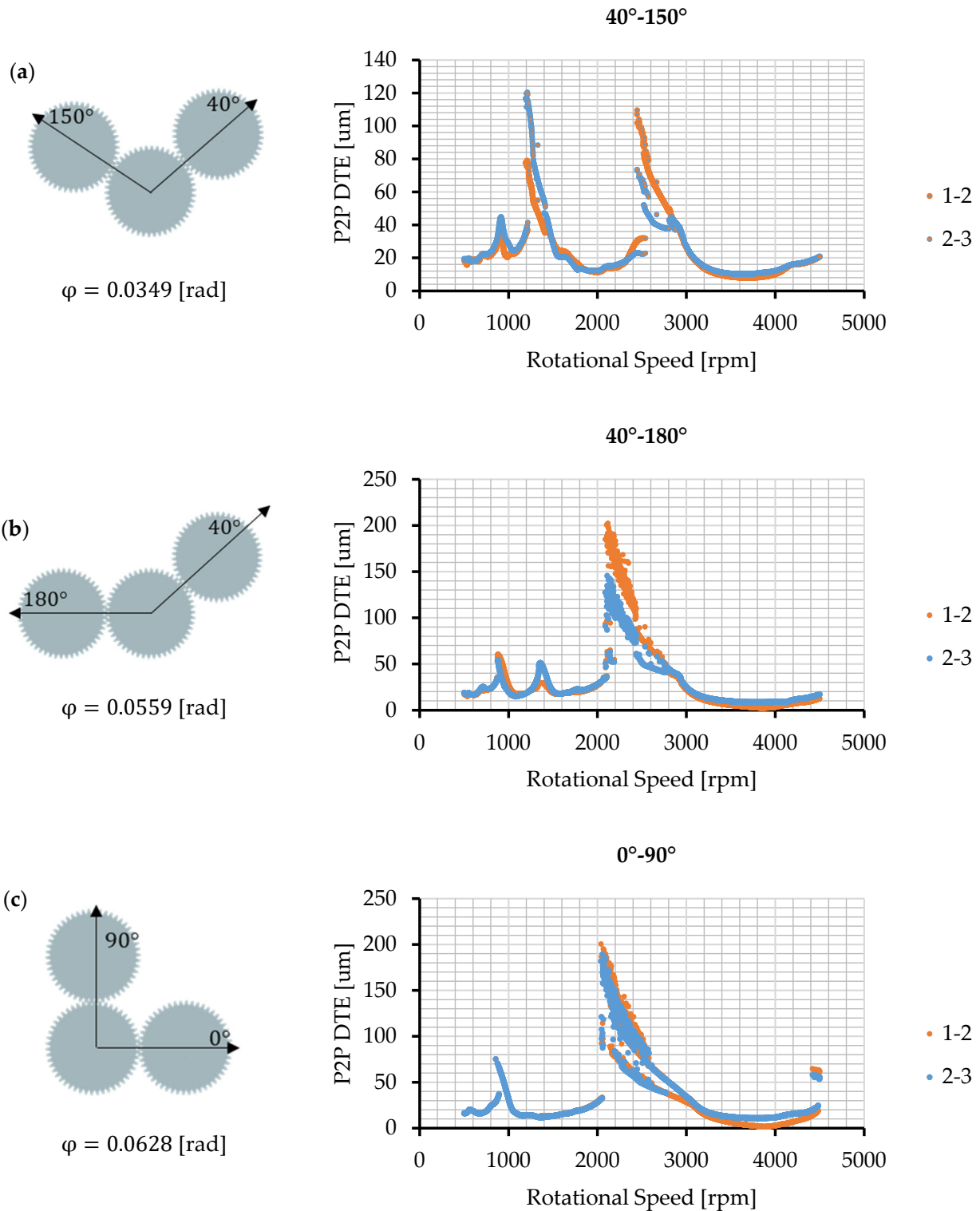


Figure 10. Cont.

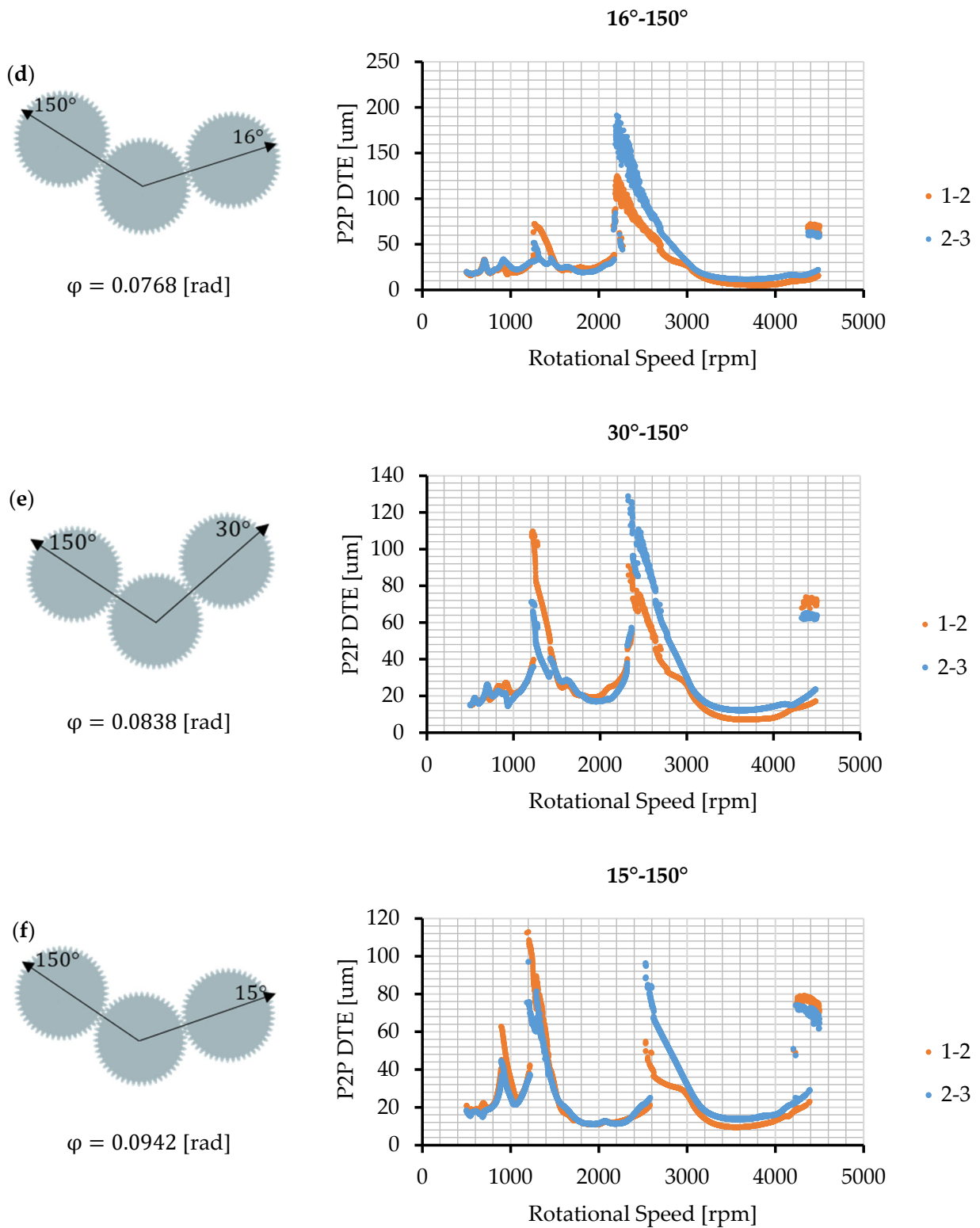
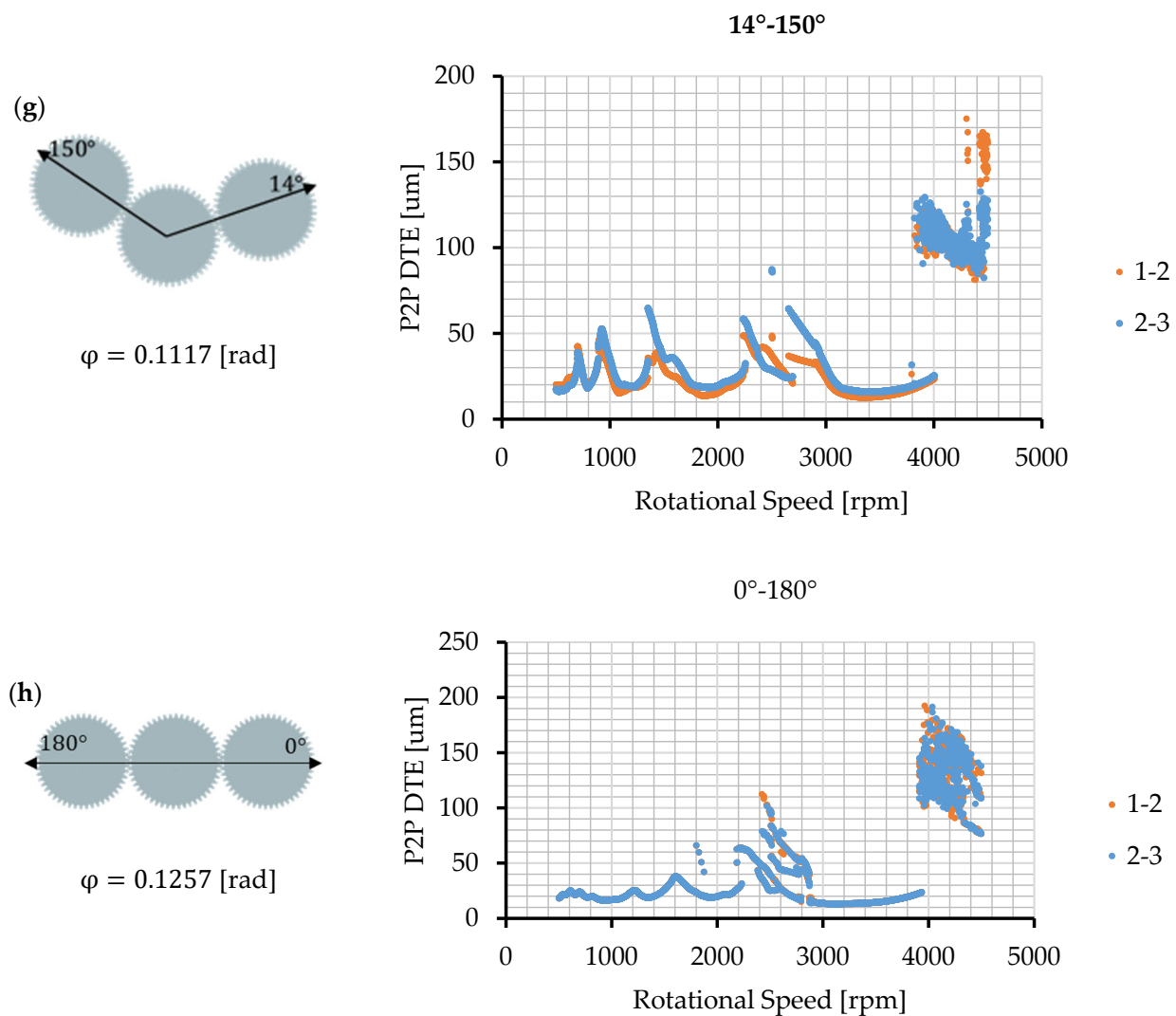


Figure 10. Cont.





**Figure 10.** DTE results in different gear positions. (a) 40–150°. (b) 40–180°. (c) 0–90°. (d) 16–150°. (e) 30–150°. (f) 15–150°. (g) 14–150°. (h) 0–180°.

The phase difference between gears coming into contact directly changes the frequency ranges and amplitudes of harmonics and sub-harmonics. This study is performed by defining a rotational speed-dependent time between gear mesh stiffness. The position angles of the gear pairs are transformed into phase differences using analytical geometry relations. Different gear position angles are evaluated such that the phase difference can be between 0 and a maximum of 0.1257 [rad]. As mentioned before, the same gear parameters are used for 1–2 and 2–3 gear pairs from Ref [23] with 340 Nm torque input to determine the effect of the phase difference in the torque split model on the system's dynamic response. Peak-to-peak DTE and gear position graphs between phase differences of 0.0349 [rad] at 40–150°, 0.0559 [rad] at 40–180°, 0.0628 [rad] at 0–90°, 0.0768 [rad] at 16–150°, 0.0838 [rad] at 30–150°, 0.0942 [rad] at 15–150°, 0.1117 [rad] at 14–180°, and 0.1257 [rad] at 0–180° are shown in Figure 10 for the torque split model with the given same gear parameters.

As can be seen in Figure 10, the results are not the same as obtained in the 1–2 and 2–3 gear pairs. The magnitude and frequency of subharmonics also vary. Although the magnitude of subharmonics decreased in some gear pairs, DTE values increased in general due to the second gear pair excitation. Meanwhile, with a phase difference of 0.0349 [rad], the amplitude of the subharmonic at 1200 [rpm] increases, the amplitude at 2200 [rpm] increases between 0.0559 [rad] and 0.0738 [rad], and the amplitude of other harmonics decreases slightly. The amplitude value at 2000–2200 [rpm] is relatively less than the phase

difference between 0.0559 and 0.0738 [rad] for phase differences between 0.0838 [rad] and 0.0942 [rad]. Accordingly, there is a more stable system response in this frequency range. Instability is seen at 0.1117 and 0.1257 [rad] phase differences and a 4000 [rpm] rotational speed.

When the system responses of each phase difference are examined, especially for 0–4000 [rpm] rotational speed, the system is more stable at phase differences between 0.0349 [rad] and 0.0838–0.0942 [rad]. Therefore, optimization of the phase in the design may reduce vibration and noise. In the example of the torque split gear system, positioning using the same phase difference in the 0–90 gear position can achieve a better result in terms of vibration at an operating speed of 1200–1500 [rpm].

### 3.2. Contact Pressure Distribution in the Torque Split Model

In the proposed model, the components in the line of action direction of the separating elements from each contact on the tooth surface are combined. These amounts of deformation can cause non-uniform loaded tooth contact and partial loss of contact on the tooth surface. In this study, which is conducted using the parameters of Table 1, a smoother transition in the roll angle is also achieved by applying a 5  $\mu\text{m}$  tip relief.

The load distribution algorithm used in this study is validated using the ANSYS® finite element program. The steps followed in the finite element study are given as follows:

- 1- The material assignment is performed after adding model geometry.
- 2- Gears are positioned in a single tooth region in Figure 11.
- 3- The contact areas of the pinion and the driven gear are marked.

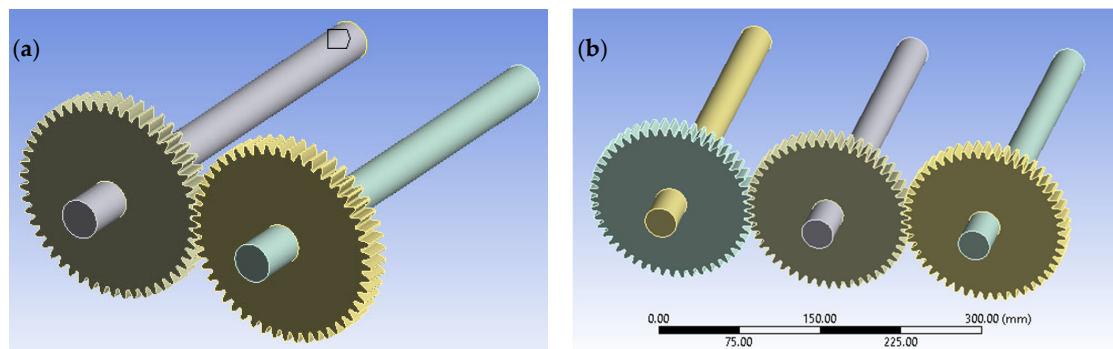


**Figure 11.** Gears in single tooth region. (a) Gear pair. (b) Torque split model.

- 4- The friction coefficient is defined as 0.05.
- 5- The ‘Augmented Lagrange’ method on contact, ‘asymmetric’ behavior, and ‘nodal-projected normal from contact’ detection method are determined.
- 6- Since the Hertz compliance is dependent on the force, its stiffness is updated in each iteration.
- 7- The mesh size of 0.06 mm in the gear contact area is used as in Figure 12. In the gear pair system, there are 4,933,469 total nodes and 3,517,393 elements. There are 10,175,252 total nodes and 7,350,662 elements in the torque split model.

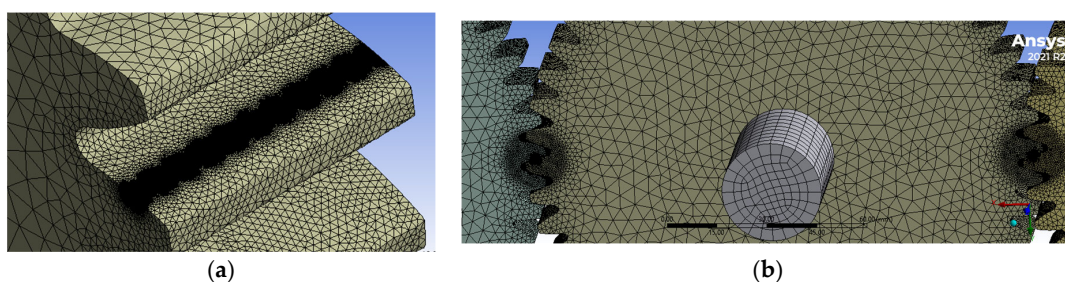


**Figure 12.** (a) Mesh structure on the gear. (b) Torque split model contact regions.

- 8- The X and Y directions are fixed at the endpoints of the shaft to provide support on the shafts. At the end where torque is applied to the pinion,  $R_x$ ,  $R_y$ , and  $R_z$  are released in Figure 13. One of both ends of the shaft is released in the Z direction. In the driven gears,  $R_z$  is fixed at the end in the direction of torque flow to simulate the torque of resistance.  $R_x$  and  $R_y$  are released. One of both ends of the shaft is released in the Z direction. X and Y coordinates represent the lateral plane and can be assumed perpendicular to the shaft axis. The shaft lays along the Z direction.

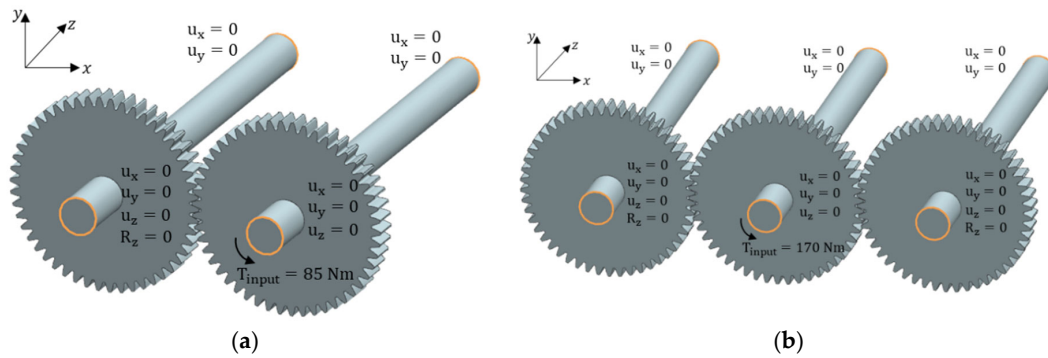


Figure 13. Boundary conditions. (a) Gear pair. (b) Torque split model.

- 9- 85 Nm torque for the gear pair and 170 Nm for the torque split are applied to the pinion from one end in a certain period and the system is loaded.

There is a 99% similarity between the analytical load distribution result as a result of the analysis performed in the single tooth region with the ANSYS® finite element software given in Figure 14a1,a2. Gear contact loss is approximately half of the face width in the gear pair contact analysis.

The maximum pressure is 714 [MPa] in the torque split analytical model and 720 [MPa] in the finite element model as shown in Figure 14a1,a2. In the torque split model, the results at different gear position angles are studied using the analytical approach given in this study. The maximum pressure is 614 [MPa] in the torque split analytical model and 580 [MPa] in the finite element model as shown in Figure 14b1,b2. In the torque split model, contact loss is observed at approximately 1–2 mm. The amount of loss is approximately at this level in the finite element model.

The pinion location is taken as the reference point, and the effect of the angle between the gears on the contact pressure with the asymmetrical positioning is shown at 0–180°, 40–180°, 0–150°, and 0–90° angles in the pressure distribution in Figure 15. In this gear position, since the line of action is opposite in both gears that transmit torque from the pinion, the deflection of the pinion shaft is negligible. It can be said that only the shaft deflections of the driven gears affect the contact pattern. The distribution in Figure 15a1–a3 with 180° phase difference and asymmetric gear positioning is the case with the least contact loss.

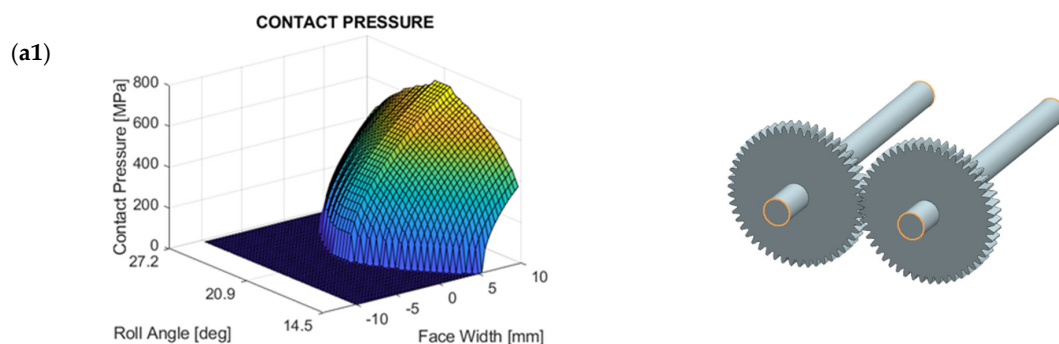
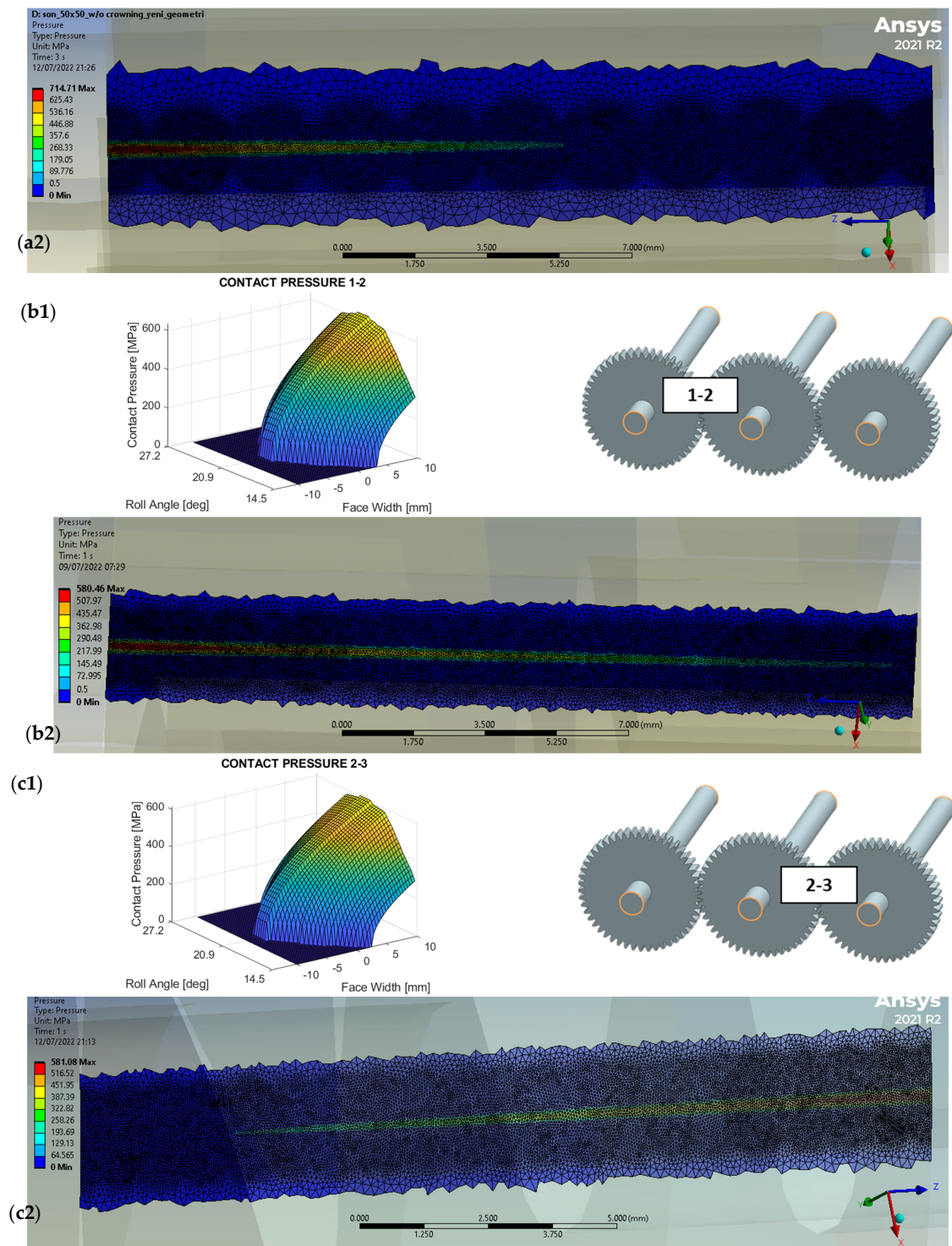
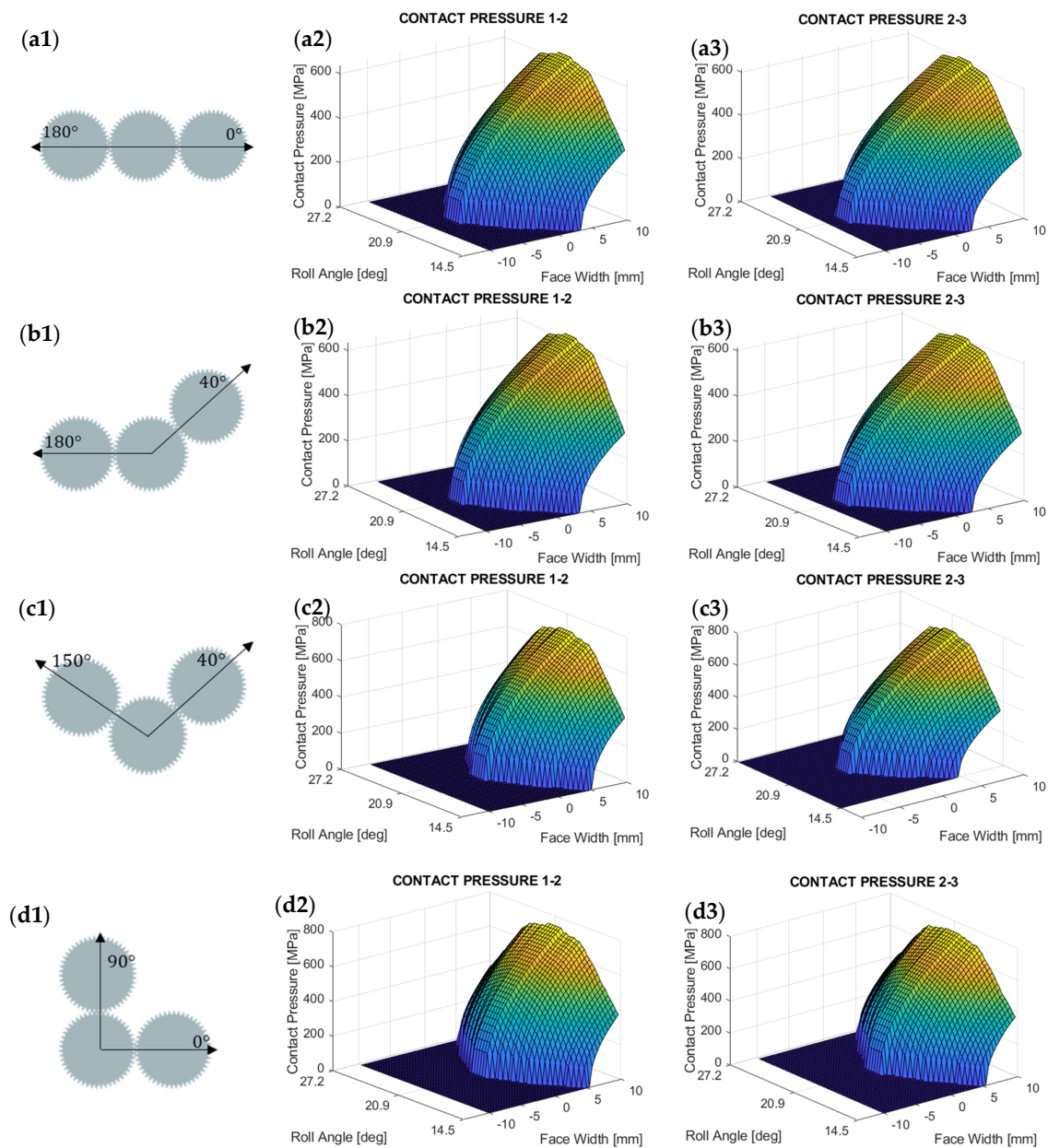


Figure 14. Cont.



**Figure 14.** The proposed analytical method comparison with finite element model (a1,a2) Gear pair. (b1,b2) Torque split 1–2 gear pair. (c1,c2) Torque split 2–3 gear pair.



**Figure 15.** Contact pressure distribution in gear pairs 1–2 and 2–3, respectively. (a1–a3) 0–180° positions. (b1–b3) 40–180° positions. (c1–c3) 40–150° positions. (d1–d3) 0–90° positions.

The angle difference of 1–2 and 2–3 gear pairs decreases at 40–180° positions, and with this positioning in Figure 15b1–b3, the contact loss slightly increased. The difference in pressure distribution between the two gear pairs is due to the inclusion of the weight effect in the calculated model.

The pressure distribution at the 40–150° position is examined in Figure 15c1–c3. Since the phase difference is less than in the previous example, the maximum contact force value increased while the partial contact loss increased as expected.

The 0–90° positioned torque split model is studied in Figure 15d1–d3, which has the biggest phase difference compared to others and shows the highest contact loss. Shaft bending in the pinion is close to the deflection of the driven gears. The contact pressure or partial contact loss between gears 1–2 and 2–3 is very close. As a result, the pressure distribution in the gear pairs according to the position does not seem different if the weight effect is neglected.

#### 4. Conclusions

An analytical model was proposed for the gear positions and phase difference to numerically calculate the system dynamic response in the torque split gear model, which is especially used in cases such as driving two separate pieces of equipment. Shaft bending and torsional deformation of the gear body were studied, and the calculations were validated by the finite element method for the pressure distribution algorithm, similar to the method in the AGMA 927 standard. The direction of the force in the pinion is determined by the reaction forces in the driven gears to calculate the load distribution in the torque split model. The main outcomes can be given as follows:

- The direction of the shaft bending in the pinion and the load distribution algorithm are calculated for each gear pair. There is the least reaction force compared to the  $0^{\circ}$ – $180^{\circ}$  positioning in the torque split model, while as this angle decreases, the reaction force increases in the pinion, and the partial tooth contact loss increases.
- The angle between gears directly affects the phase difference. The difference in the roll angle between gears coming into contact is reflected in the dynamic model as a phase delay. Different dynamic transmission error results occur in gear pairs even if gears with the same tooth number are used in the torque split model.
- Since the phase difference changes according to parameters such as the number of teeth and the gear position angle, the effect on the dynamic transmission error in the gears is obtained by modeling each of them. The positioning of gears can cause instability in the harmonics of the torque split model. It is possible to obtain a lower DTE amplitude depending on the location at various operating speed ranges.

The gear parameters are taken as the same and the gear contact is assumed to be uniformly loaded to determine the effect of the phase difference directly. As a result of the asymmetrical positioning of the gear on the shaft, the mesh stiffness of the gear pair changes with partial loss of contact. In a gear pair design with a relatively long shaft, the shaft deflection effect can be reduced by placing the gear in the center of the shaft. In systems such as the torque split model, the effect of shaft deflection can be compensated by positioning the driven gears at an appropriate angle with respect to the drive gear. In the next study, establishing the dynamic model at different phase angles with the gears positioned asymmetrically on the shaft and examining the system responses is planned.

**Author Contributions:** S.E.C.: Investigation, writing—original draft. C.D.: Finite element analysis, supervision, review and editing. All authors have read and agreed to the published version of the manuscript.

**Funding:** This research received no external funding.

**Institutional Review Board Statement:** Not applicable.

**Informed Consent Statement:** Not applicable.

**Data Availability Statement:** The datasets generated during the current study are not publicly available. Because the generated MATLAB code may be used for another study, it is available from the corresponding author upon reasonable request.

**Conflicts of Interest:** The authors declare that they have no known competing financial interests or personal relationships that could have appeared to influence the work reported in this paper.

Appendix A

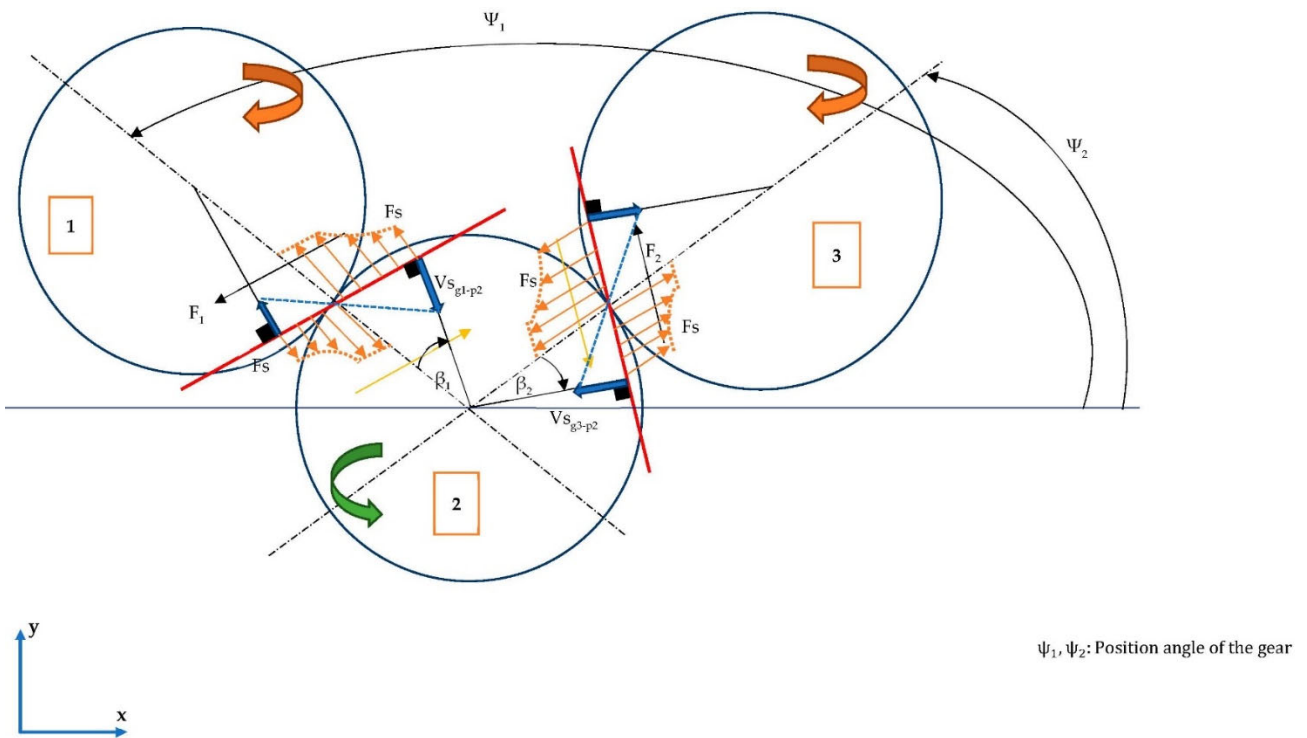


Figure A1. The friction force direction determination.

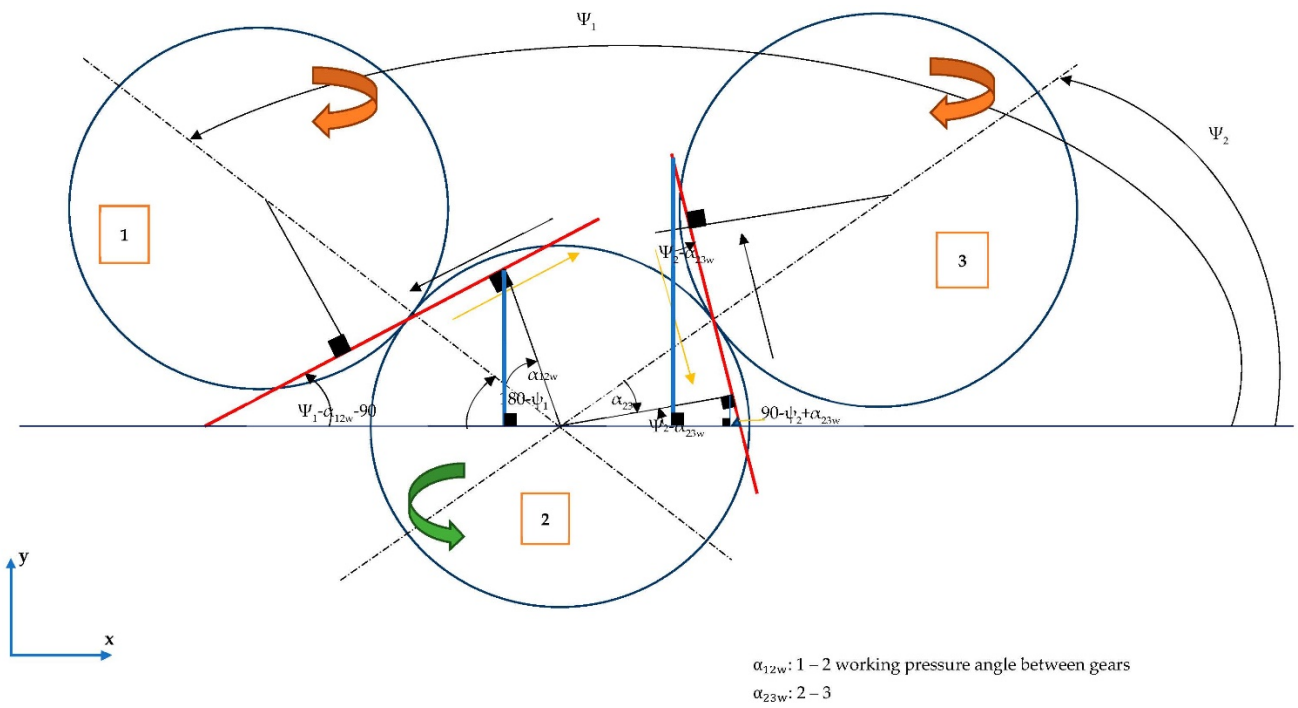


Figure A2. Determining the angles to the line of action direction in the torque split model.

## References

1. Eritenel, T.; Parker, R.G. An investigation of tooth mesh nonlinearity and partial contact loss in gear pairs using a lumped-parameter model. *Mech. Mach. Theory* **2012**, *56*, 28–51. [[CrossRef](#)]
2. Yuan, B.; Chang, S.; Liu, G.; Chang, L.; Liu, L. Quasi-static analysis based on generalized loaded static transmission error and dynamic investigation of wide-faced cylindrical geared rotor systems. *Mech. Mach. Theory* **2019**, *134*, 74–94. [[CrossRef](#)]
3. Yuan, B.; Chang, L.; Liu, G.; Chang, S.; Liu, L.; Shen, Y. An efficient three-dimensional dynamic contact model for cylindrical gear pairs with distributed tooth flank errors. *Mech. Mach. Theory* **2020**, *152*, 103930. [[CrossRef](#)]
4. Wang, Q.; Xu, K.; Huai, T.; Ma, H.; Wang, K. A mesh stiffness method using slice coupling for spur gear pairs with misalignment and lead crown relief. *Appl. Math. Model.* **2021**, *90*, 845–861. [[CrossRef](#)]
5. Kahraman, A.; Nevzatoglu, H.; Houser, D.R.; Zakrajsek, J.J. Dynamic analysis of geared rotors by finite elements. *J. Mech. Des. Trans. ASME* **1992**, *114*, 507–514. [[CrossRef](#)]
6. Ma, H.; Pang, X.; Feng, R.; Wen, B. Evaluation of optimum profile modification curves of profile shifted spur gears based on vibration responses. *Mech. Syst. Signal Process.* **2016**, *70–71*, 1131–1149. [[CrossRef](#)]
7. Dai, X.; Cooley, C.G.; Parker, R.G. An Efficient Hybrid Analytical-Computational Method for Nonlinear Vibration of Spur Gear Pairs. *J. Vib. Acoust. Trans. ASME* **2019**, *141*, 011006. [[CrossRef](#)]
8. Han, G.; Yuan, B.; Qiao, G. Tooth Surface Modification for Helical Gear Pairs considering Mesh Misalignment Tolerance. *Shock Vib.* **2021**, *2021*, 5563648. [[CrossRef](#)]
9. Xiang, L.; Gao, N. Coupled torsion-bending dynamic analysis of a gear-rotor-bearing system with eccentricity fluctuation. *Appl. Math. Model.* **2017**, *50*, 569–584. [[CrossRef](#)]
10. Inalpolat, M.; Handschuh, M.; Kahraman, A. Influence of indexing errors on dynamic response of spur gear pairs. *Mech. Syst. Signal Process.* **2015**, *60*, 391–405. [[CrossRef](#)]
11. Bonori, G.; Pellicano, F. Non-smooth dynamics of spur gears with manufacturing errors. *J. Sound Vib.* **2017**, *306*, 271–283. [[CrossRef](#)]
12. Ghosh, S.S.; Chakraborty, G. On optimal tooth profile modification for reduction of vibration and noise in spur gear pairs. *Mech. Mach. Theory* **2016**, *105*, 145–163. [[CrossRef](#)]
13. Kahraman, A. Dynamic analysis of a multi-mesh helical gear train. *J. Mech. Des. Trans. ASME* **1994**, *116*, 706–712. [[CrossRef](#)]
14. Chen, Y.; Zhu, R.; Jin, G.; Xiong, Y.; Gao, J.; Liao, M. A new mathematical modeling method for four-stage helicopter main gearbox and dynamic response optimization. *Complexity* **2019**, *2019*, 5274712. [[CrossRef](#)]
15. Sainte-marie, N. A Transmission-Error-Based Gear Dynamic Model: Applications to Single- and Multi-Mesh Transmissions—Applications to Single- and Multi-Mesh Transmissions. Ph.D. Thesis, Université de Lyon, Lyon, France, 2016.
16. Brethee, K.F.; Zhen, D.; Gu, F.; Ball, A.D. Helical gear wear monitoring: Modelling and experimental validation. *Mech. Mach. Theory* **2017**, *117*, 210–229. [[CrossRef](#)]
17. Al-Shyyab, A.; Kahraman, A. Non-linear dynamic analysis of a multi-mesh gear train using multi-term harmonic balance method: Sub-harmonic motions. *J. Sound Vib.* **2005**, *279*, 417–451. [[CrossRef](#)]
18. Yavuz, S.D.; Saribay, Z.B.; Cigeroglu, E. Nonlinear time-varying dynamic analysis of a multi-mesh spur gear train. *Conf. Proc. Soc. Exp. Mech. Ser.* **2016**, *4*, 309–321.
19. Walha, L.; Fakhfakh, T.; Haddar, M. Nonlinear dynamics of a two-stage gear system with mesh stiffness fluctuation, bearing flexibility and backlash. *Mech. Mach. Theory* **2019**, *44*, 1058–1069. [[CrossRef](#)]
20. Shi, J.; Gou, X.; Zhu, L. Modeling and analysis of a spur gear pair considering multi-state mesh with time-varying parameters and backlash. *Mech. Mach. Theory* **2019**, *134*, 582–603. [[CrossRef](#)]
21. Kim, W.; Yoo, H.H.; Chung, J. Dynamic analysis for a pair of spur gears with translational motion due to bearing deformation. *J. Sound Vib.* **2010**, *329*, 4409–4421. [[CrossRef](#)]
22. Gonzalez-Perez, I.; Roda-Casanova, V.; Fuentes, A. Modified geometry of spur gear drive for compensation of shaft deflections. *Meccanica* **2015**, *50*, 1855–1867. [[CrossRef](#)]
23. Blankenship, G.W.; Kahraman, A. Steady state forced response of a mechanical oscillator with combined parametric excitation and clearance type non-linearity. *J. Sound Vib.* **1995**, *185*, 743–765. [[CrossRef](#)]
24. *Standard AGMA 927-A01; Load Distribution Factors—Analytical Methods for Cylindrical Gears.* American Gear Manufacturer Association: Alexandria, VA, USA, 2018.
25. *Standard AGMA 908-B89; Geometry Factors for Determining the Pitting Resistance and Bending Strength of Spur, Helical and Herringbone Gear Teeth.* American Gear Manufacturers Association: Alexandria, VA, USA, 2020.
26. Kang, M.R.; Kahraman, A. Measurement of vibratory motions of gears supported by compliant shafts. *Mech. Syst. Signal Process.* **1999**, *29*, 391–403. [[CrossRef](#)]
27. Tatar, A. Effect of Planetary Gearboxes on the Dynamics of Rotating Systems. Ph.D. Thesis, Imperial College, London, UK, 2019.
28. Hua, X.; Lim, T.; Peng, T.; Wali, W. Dynamic analysis of spiral bevel geared rotor systems applying finite elements and enhanced lumped parameters. *Int. J. Automot. Technol.* **2012**, *13*, 97–107. [[CrossRef](#)]